NASA Technical Memorandum 108998

Sampling and Position Effects in the Electronically Steered Thinned Array Radiometer (ESTAR)

Stephen J. Katzberg

August 1993

National Aeronautics and Space Administration

Langley Research Center
Hampton, Virginia 23681-0001

Sampling and Position Effects in the Electronically Steered Thinned Array Radiometer (ESTAR)

Introduction

Microwave radiometers have been successfully utilized in the past to provide environmental information not obtainable from any other source. Salinity, soil moisture, ice concentration, percent open water, rainfall, sea surface temperature, and water vapor are examples of the type of information available.

Unfortunately for practical remote sensing applications, the microwave techniques require the use of relatively large antennas to provide good surface spatial resolution.

Microwave radiometers have a significant advantage over most optical sensors. The microwave radiometers detect signals as a superposition of voltages resulting from received electromagnetic fields. The voltages are stochastic and are generally converted to power by non-linear detection. Optical signals on the other hand are almost exclusively detected as a received power that generates a charge carrier electric current. Coherent summing is not readily possible for optical signals, while it is possible for microwave.

Thus, radio interferometry can be implemented to realize some objective, such as increased resolution. Astronomical radio telescopes utilize coherent techniques to increase resolution available from a single telescope without having to resort to building less practical, much larger structures. In effect, a synthetic aperture is realized.

An environmental remote sensing extension of coherent summing has been proposed called the ESTAR, Electronically Steered Thinned Array (References 1,2,and 3). In this implementation, a single line, parallel lines, or two orthogonal linear antenna arrays are utilized. Crosscorrelation of the radio frequency signals from pairs of antenna elements generate samples of the Fourier transform of the remote source radiated energy.
It is the purpose of this paper to develop a simple model of the ESTAR concept which is complete enough to allow engineers to assess the impacts of practical considerations that arise during hardware design phases.

The ESTAR Data Generation

The ESTAR model to be analyzed in this paper is one in which the antenna "farm" is a perpendicular pair of linear arrays with two different numbers of equally spaced elements in each array, N and M. Note that the antenna at the intersection of the two orthogonal arms may be shared by both arms of the antenna. It will also be assumed that the ESTAR is carried on some platform such as an aircraft, a spacecraft, or balloon. Direction along the flight direction will be ξ, while direction transverse to the flight direction will be η. On the ground, direction along the flight direction will be "x" and the transverse direction will be taken to be "y." These coordinates are illustrated in Figure 1. Utilizing the Huygens-Fresnel principle, (see Reference 4) it will be assumed that the superposition of the stochastic fields from an extended source is weighted by an exponential phase factor dependent on the distance between source and antenna point. The obliquity factor is assumed unity:

$$(1) \qquad \mathcal{E}(\xi,\eta,t) = \int \hat{a}(t-r/c)\frac{\exp(ikr)\ \mathcal{E}(x,y)}{ir\lambda}\,dxdy$$

where $k=2\pi/\lambda$ and r is the distance between a point x,y at the remote source and ξ, η a point at the antenna array.

To develop the approximations that yield the basis for the ESTAR concept, it is necessary to make the Fraunhoffer approximation to the Huygens-Fresnel formulation above. The variable r in terms of the source and antenna coordinates can be written:

$$(2) \qquad r = \left((x-\xi)^2 + (y-\eta)^2 + h^2\right)^{1/2}$$

Because the ESTAR application is assumed to be a remote sensing one, the distance from the source (approximate) plane to the antenna plane, h, can be factored out:

$$(3) \qquad r = h\left(\frac{(x-\xi)^2}{h^2} + \frac{(y-\eta)^2}{h^2} + 1\right)^{1/2}$$

Under the assumption that h is much larger than the other variables (a consideration to be reassessed later), the

Fresnel approximation results:

$$(4) \qquad r = h + \frac{\xi x}{h} + \frac{\eta y}{h} + \frac{x^2 + y^2}{2h} + \frac{\xi^2 + \eta^2}{2h}$$

If the further assumption is made that quadratic terms in x,y, ξ,η, can be dropped, the Fraunhoffer formulation results:

$$(5) \qquad r = h + \frac{\xi x}{h} + \frac{\eta y}{h}$$

Inserting this value for r in the Huygens-Fresnel integral yields the form that will be used to give the basis for the ESTAR analysis:

$$(6) \qquad \hat{S}(\xi,\eta,t) = \int S(x,y,t)\ \exp\left[-2\pi i\left(h^2 + \xi x + \eta y\right)/\lambda h\right]\ dxdy$$

Where now, other than the constant phase factor $\exp(2\pi ih/\lambda)$, the integral is the Fourier transform of the source electric field strength.

In the ESTAR concept, the desire is to determine various Fourier transform samples in order to reconstruct, via an inverse transform, the source radiation characteristics. To do this the ESTAR concept crosscorrelates the signals from the various antenna elements:

$$(7) \qquad R(\xi,\eta,\xi',\eta') = \left\langle S(\xi,\eta,t)^{*}\, S(\xi',\eta',t)\right\rangle$$

Or, rewriting this in terms of the field strength at the antenna plane (dropping the explicit time dependence for convenience):

$$(8)\quad R(\xi,\eta,\xi',\eta') = \int \left\langle S^{*}(x,y)\quad S(x',y') \right\rangle \exp\left[-2\pi i(\xi x'-\xi' x+\eta y'-\eta' y)/\lambda h\right] dx'dxdy'dy$$

Because the source is assumed to be incoherent, the radiation field only correlates when originating from the same point:

$$(9)\quad \left\langle S^{*}(x,y)S(x',y') \right\rangle = |S(x,y)|^{2}\,\delta(x-x')\delta(y-y')$$

This then yields the following expression for the detected signal:

$$(10)\quad R(\xi,\eta,\xi',\eta') = \int |S(x,y)|^{2} \exp\left[-2\pi i((\xi-\xi')x+(\eta-\eta')y)/\lambda h\right]dxdy$$

Where it can now be recognized that the cross-correlation yields the two-dimensional spatial Fourier transform of the source "intensity" evaluated at the spatial frequencies of:

$$(11a)\quad k_{\xi} = \frac{2\pi(\xi-\xi')}{h\lambda}$$

$$(11b)\quad k_{\eta} = \frac{2\pi(\eta-\eta')}{h\lambda}$$

Note that the constant phase factor has gone and that the spatial frequencies are set by the difference in distance between the elements being cross-correlated. From this result it can be seen that the highest spatial frequency that can be determined along one transform axis is:

$$(12) \quad k_{max} = \frac{2\pi(N-1)l}{\lambda h}$$

where l is the antenna spacing and M is the number of elements along ξ and N is the number along η.

The lowest frequency, other than zero, is:

$$(13) \quad k_{min} = \frac{2\pi l}{\lambda h}$$

Thus, there are samples of the Fourier transform that cover the range:

$$(14) \quad 0, \frac{2\pi l}{\lambda h} \leq k \leq \frac{2\pi(N-1)l}{\lambda h}$$

In effect, the data derived at each transform sample is equivalent to multiplying the source (ground, ocean, etc.) intensity function by a set of sinusoids at discrete frequencies. The more densely spaced and extensive, the better will be the ability to reconstruct the original distribution.

The Transform Pair Relationship

It is important to clearly determine the relationship between the variables associated with the source plane and the antenna plane and the transform variable. Note that in the equations above, the exponential transform kernel includes more than just x,y,ξ, and η. Aside from the factor of 2π there is division by the product h and λ. The question arises to which variables to associate which part of the dividend? The answer depends on what objective is in mind, although the result will be correct for whatever choice.

To see the relationship, suppose there is a sinusoidal intensity pattern at the antenna plane with "period" L. Since the intensity pattern is related to a source radiation pattern through the Fourier transform, it remains to determine what relationship there is between the two. Since the Fourier transform of the sinusoid is a pair of delta functions and the shorter the "period", the larger the associated "frequency" it remains to

determine what the scale factor is. Knowing the "period" in terms of ξ the transform variable can be found by dividing by h and λ to make the form compatible with the transform kernel. Thus, a "period" L becomes the transform variable "period" $L/h \cdot \lambda$.

The delta function transform then can be identified to be at locations $+h \cdot \lambda/L$ and $-h \cdot \lambda/L$ in the source plane. Conversely, a sinusoid in the source plane of "period" L' can be identified with a pair of delta functions located at ξ values of $\pm h \cdot \lambda/L'$.

Aliasing

A considerable worry that must accompany any sampled system is the concern over aliasing from undersampling or insufficient bandlimiting. In the ESTAR case, the Fourier transform is that which is sampled and the concern is whether or not aliasing artifacts will be present that compromise the source intensity reconstruction. Sampling the Fourier transform sufficiently allows its perfect reconstruction from which the reconstruction of the source can be had. Analysis of the sampling process takes the form of assessing the apparent source characteristics derived from the possibly imperfectly sampled antenna signals.

From the earlier discussion on the relation of transform variables to antenna and source coordinates, it is fairly easy, if a little confusing, to address the degree of aliasing. With the antenna spacing of 1, it is clear that the largest antenna size that can exist without overlapping is also 1. Assuming that the far-field pattern from a circular aperture antenna of diameter "w" ($\leq$1) is an Airy pattern illustrated in Figure 2, whose first zero in the source plane is at $1.22 \cdot h \cdot \lambda/w$. For a sampling interval of 1, the replication of images of the sampled data will occur at "frequencies" in the source plane at $h \cdot \lambda/1$. Also illustrated in Figure 2 is the replication of the Airy pattern with these values of sampling interval and assuming an antenna diameter of "w" as discussed above. Thus, the maximum bandlimiting that could be done simply by increasing antenna size to the largest physical size will not constrain the source signal distribution to below on half the replication interval, and severe aliasing must occur. Moreover, if the antennas are smaller than the maximum possible, the aliasing must be aggravated all the more. Note that this effect is one from the mathematics of the sampling process and does not disappear because it happens outside the field-of-view as discussed in Reference 1.

It may be possible to improve the aliasing rejection by properly phasing and adding the signal from adjacent pairs of antennas and then cross-correlating for the output signals based on the new pairs. Further analysis might prove this to be a reasonable approach, but it is clear that some approach must be found to avoid major image contamination.

Number of Available Samples

It is useful to determine how many samples of each spatial frequency are available, a question of importance to signal-to-noise assessment for example. It also makes it possible to compare the ESTAR concept to the result that would be achieved by a filled array.

Table I shows the number of available samples for each Fourier component. In principle all equivalent cross- correlations would be added together to improve the signal- to-noise. Conversely, where signal-to-noise is abundant, the samples might be adjusted for some other objective, such as frequency response leveling.

From the Table it is possible to see that along the transform axes, the ESTAR has strong sampling at the lower frequencies, tapering off to one sample at the highest frequency. Off the transform axes, there exists one, and only one sample at each frequency point. A two dimensional illustration of this sampling lattice is shown in Figure 3. The lattice gives an impression of being two orthogonal mountain ranges with the peak for each at their intersection. The off-axis samples are a thin uniformly spaced forest with each element of unit height filling the rest of the plane.

The effect of having a filled aperture might be thought of as replicating the antenna array and then rotating it. In the transform domain, the effect would be similar, giving a replication and then a rotation, ultimately filling the entire plane. The resultant response function would then look cone-like. That this is so follows from the fact that the process of cross-correlating signals from the various antenna elements is similar to the effect that the finite aperture of a parabolic antenna has on the signal intensity. For a point source, the magnitude of the field and intensity distributions at the aperture are constant (Fourier transform of a delta function.) Only that limited spatial part in the aperture is collected, however. Since intensity is the squared modulus of field strength, the result is equivalent to the transform of the autocorrelation of the aperture transmittance. Because the aperture is an open hole with unity transmittance, the autocorrelation will have a cone-like characteristic.

The effect that the sampling pattern has on the image must be such that a much better representation of the Fourier transform can be made for Fourier components along the axes than in the much larger areas away from the axes. The sparse sampling off-axis means that there are concerns for sufficient sampling (Nyquist rate) and sensitivities to errors at these sample points.

Effect of Antenna Element Displacements

Each antenna element will suffer misplacement arising from some mechanical assembly defect, structural dynamics effect, or deployment operation. The misplacement may be larger or smaller as the case may be, but it will be assumed here that the antenna element has suffered a displacement small enough to be considered a normal preparation for operation. As shown in the section concerning the number of available samples at each frequency, some frequencies are sampled only once, while others, arising from a large number of redundant antenna pairs are taken many times. It would seem that an averaging process would help submerge the errors of highly redundant samples, while the single antenna pairs are highly susceptible to contaminating their associated frequency. Additionally, the fine structure in the desired image, which arises from the high frequencies at the antenna plane comes from just this weakly redundant set.

If, for the above reasons, the high frequency elements receive closest scrutiny, then it is to the outer antenna elements that most attention will be given. Assuming for the moment that the antenna element is displaced a vectorial distance r from where it should be. The ξ, η, and ζ distances will cause an error in the generated Fourier transform.

In order to give a simple model of the misplacement effect, it will be assumed that the error from the correct location is small with respect to the element-to-element spacing, l.
If it is assumed that the incorrect sample is separated from the correct set and a correct sample is both added and subtracted, then the effect of the incorrect sample can be given a fairly simple interpretation:

$$\hat{S}_{\varepsilon}(\xi,\eta) = \int S(x,y)\left\{\exp\left[-2\pi i\left(h^2+\zeta h + (\xi+\Xi)x+(\eta+H)y\right)/\lambda h\right] - \exp\left[-2\pi i\left(h^2+\xi x+\eta y\right)/\lambda h\right]\right\}dxdy + \hat{S}(\xi,\eta) \quad (15)$$

A final conversion can be made by recalling the is a result of the relationship between the derivative of a function and its Fourier transform (Reference 5.) It can be seen that in the case of a small displacement, the effect is approximately the same as adding a phase shifted value of the frequency sample plus a transformed "x" derivative sample, and a transformed "y" derivative sample.

$$(16) \quad \hat{S}_{\varepsilon}(\xi,\eta) = (2\pi i\zeta/\lambda)\ \hat{S}(\xi,\eta) + \Xi \frac{\partial}{\partial \xi}\hat{S}(\xi,\eta) + H \frac{\partial}{\partial \eta}\hat{S}(\xi,\eta) + \hat{S}(\xi,\eta)$$

As far as relative importance of the errors, the strongest sensitivity is the ζ component as can be seen by the direct proportion of ζ against the distance h. Multiplication of the transform by the constant phase factor is the same effect as a "rotation" of the Fourier transform real and imaginary components. Thus, the frequency sample with a simple vertical shift produces the effect of a noise derived from cross-coupling the real and imaginary components of the transform.

The two other errors represent an adding into the perfect samples of an attenuated piece of the ξ or η derivatives of the source scalar field transform. (The crosscorrelation to yield the intensity has the effect of replacing the scalar field strength with the field intensity, leaving the result otherwise not changed.) Given a position error ξ along the η direction and vice versa, it is clear that general position errors will yield cross-coupling of the ξ and η dependency of the Fourier transform through the derivatives. It is also interesting to note that the size of the error contribution is not dependent on the pair of antenna coordinates and, consequently, the frequency sample. Hence, as discussed earlier, the antenna redundancy of the lower frequencies helps to ameliorate the noise effects.

The farther out on the extremes of the antenna pattern the errors occur, the more transform components are affected. Thus, an error near the center of the antenna array would affect all transform components out to approximately one half the highest spatial frequency of $2\pi L/2 \cdot \lambda$. The minimum redundancy would be around N/2. Thus, the effect of the error on the overall calculated Fourier transform will be reduced by the factor N/2. In addition, random positioning errors could be expected to be uncorrelated and their effect would be reduced by the factor (N/2). On the other hand, if the misplaced element were out near the ends of the array the error would be added to elements with redundancy as low as unity. Error contributions in a flight system would most likely occur in the extremes of the antenna array and thus the problem is very likely to be most severe where the technique is most vulnerable.

Assessment of the limits to put on the out-of-position error depend on assumptions about the source intensity distribution in x and y. However, given some reasonable assumptions concerning the source distribution, the magnitude of the error contribution may then be determined for an assumed misplacement error using the above equations.

Conclusion

A simple model of the ESTAR concept has been developed to permit spacecraft engineers to assess some of the major impacts practical hardware designs may have on instrument performance. While it is not the purpose of this document to try to get at some of the more detailed characteristics of the ESTAR concept, it is believed that this report will be of use by creating an analytical model for engineering level end-to-end parametric trade-offs.

References

1. Ruf, Christopher S., Swift, Calvin T., Tanner, Alan B., and Le Vine, David M.; Interferometric Synthetic Aperture Microwave Radiometry for Remote Sensing of the Earth; IEEE Transactions on Geoscience and Remote Sensing, Vol. 26, No.5, September 1988.

2. Ruf, C.S., Tanner, A.B., and Levine, D.M.; The Electronically Steered Thinned Array Radiometer; Twenty- First International Symposium on Remote Sensing of Environment, October 26-30, 1987, Ann Arbor, Michigan.

3. Swift, Calvin T., Le Vine, David M., and Ruf, Christopher S.; Aperture Synthesis Concepts in Micorwave Remote Sensing of the Earth; IEEE Transactions on Microwave Theory and Techniques, Vol 39, No.12, December 1991.

4. Goodman, J.; Introduction to Fourier Optics; McGraw-Hill Book Co.; New York, 1968.

5. Bracewell, R.; The Fourier Transform and Its Applications;" McGraw-Hill Book Co., New York, 1965.

Frequency	Number of Samples
0	M+N-1
1	M-1,N-1
2	M-2,N-2
3	M-3,N-3
*	*
r	M-r,N-r
*	*
M-1 or N-1	1
n,m	1

Frequency=$2\pi nl/h$ or $2\pi ml/h$

Table I.-Number of Available Samples at Each Frequency

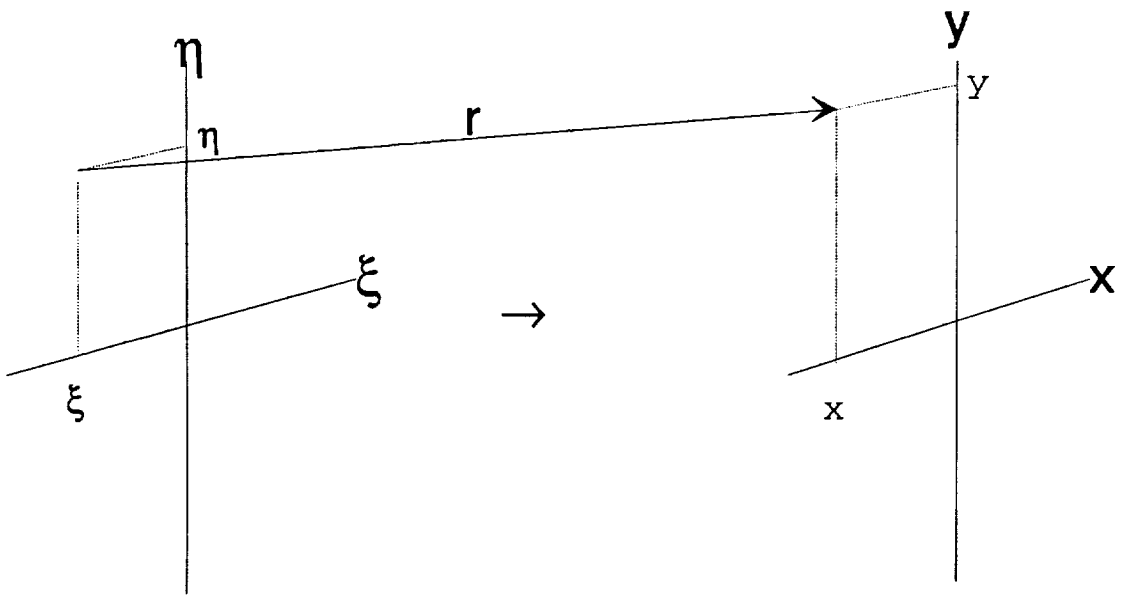

$$r = \left((x-\xi)^2 + (y-\eta)^2 + h^2\right)^{1/2}$$

$$r \cong h - \frac{\xi x + \eta y}{h} + \frac{x^2 + y^2}{2h} + \frac{\xi^2 + \eta^2}{2h}$$

Figure 1.- Coordinates for the ESTAR analysis. The Greek letters represent source coordinates and the Roman letters represent the antenna location.

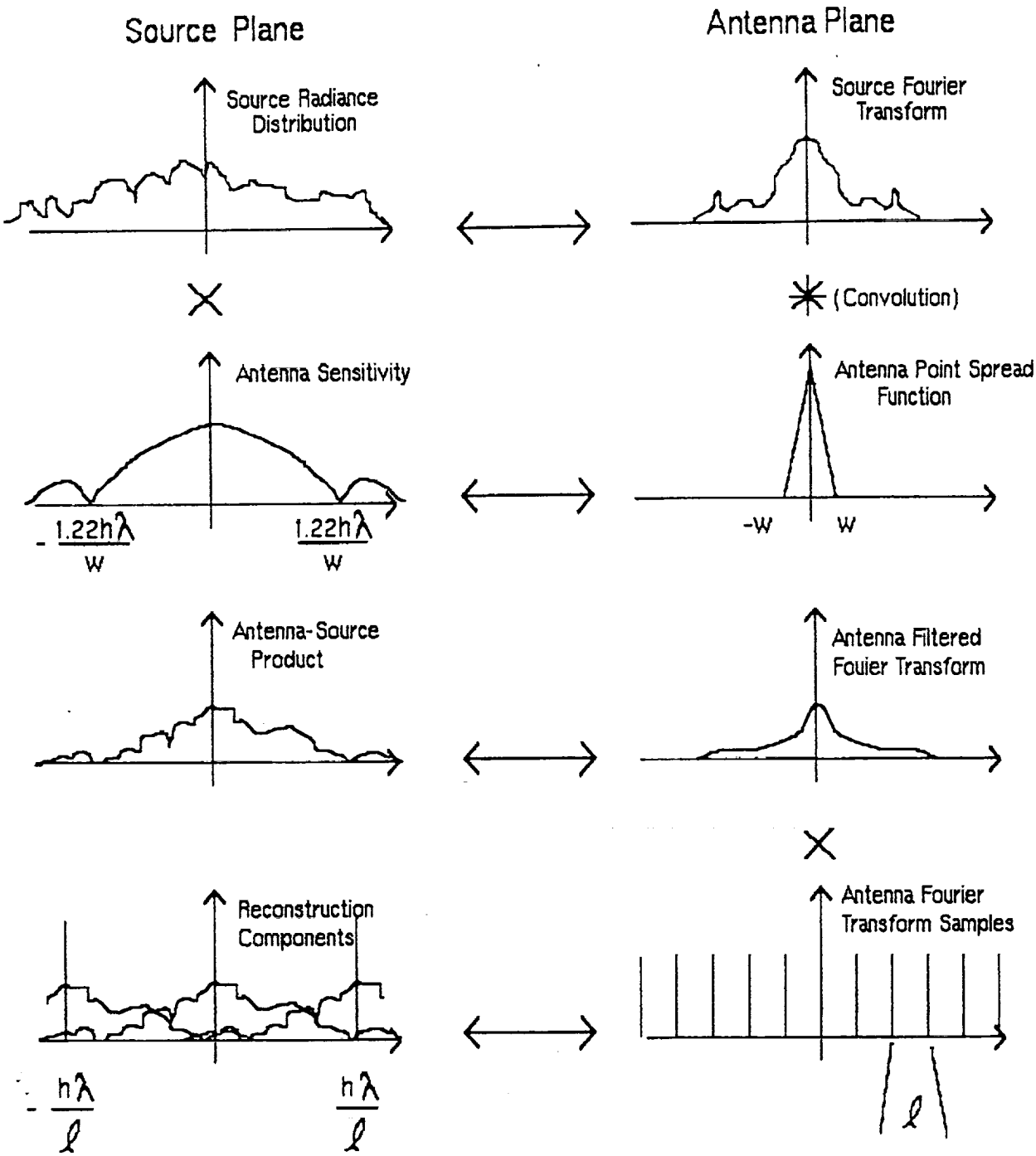

Figure 2.- Illustration of the sampling process in ESTAR showing the effects of aliasing in contaminating the Fourier transform.

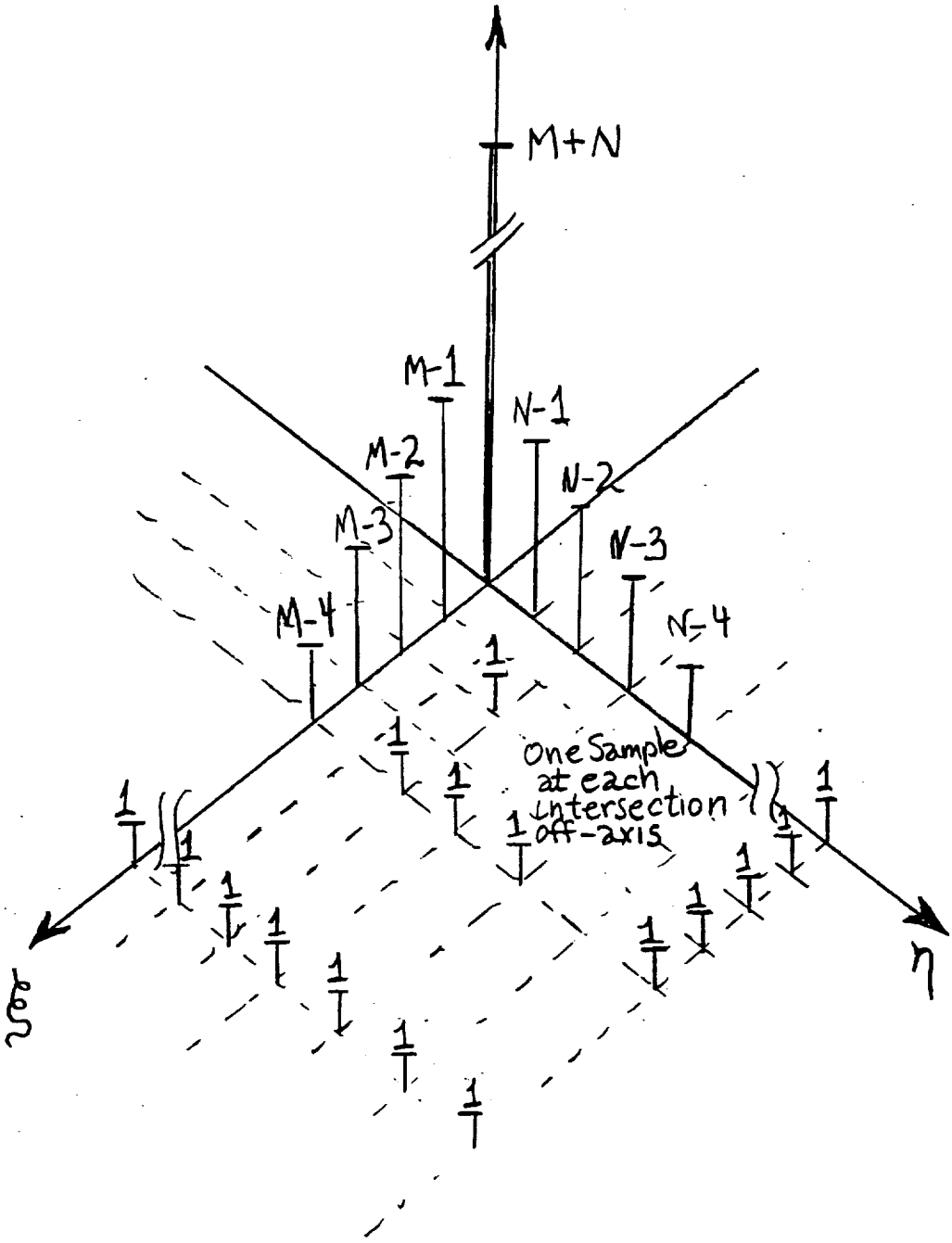

Figure 3.- Number of samples at each frequency across the two dimensional Fourier transform plane.

REPORT DOCUMENTATION PAGE

Form Approved
OMB No. 0704-0188

1. AGENCY USE ONLY *(Leave blank)*	2. REPORT DATE	3. REPORT TYPE AND DATES COVERED
	August 1993	Technical Memorandum

4. TITLE AND SUBTITLE
Sampling and Position Effects in the Electronically Steered Thinned Array radiometer (ESTAR)

5. FUNDING NUMBERS
476-14-15-01

6. AUTHOR(S) Stephen J. Katzberg

7. PERFORMING ORGANIZATION NAME(S) AND ADDRESS(ES)
NASA Langley Research Center
Hampton, VA 23681-0001

8. PERFORMING ORGANIZATION REPORT NUMBER

9. SPONSORING / MONITORING AGENCY NAME(S) AND ADDRESS(ES)
National Aeronautics and Space Administration
Washington, DC 20546-0001

10. SPONSORING / MONITORING AGENCY REPORT NUMBER
NASA TM-108998

11. SUPPLEMENTARY NOTES

12a. DISTRIBUTION / AVAILABILITY STATEMENT
Unclassified - Unlimited

Subject Category 43

12b. DISTRIBUTION CODE

13. ABSTRACT *(Maximum 200 words)*

A simple engineering level model of the Electronically Steered Thinned Array Radiometer (ESTAR) is developed that allows an identification of the major effects of the sampling process involved with this technique. It is shown that the ESTAR approach is sensitive to aliasing and has a highly non-uniform sensitivity profile. It is further shown that the ESTAR approach is strongly sensitive to position displacements of the low-density sampling antenna elements.

14. SUBJECT TERMS
ESTAR, Aliasing, Microwave Radiometers, Synthetic aperture

15. NUMBER OF PAGES
16

16. PRICE CODE
A03

17. SECURITY CLASSIFICATION OF REPORT	18. SECURITY CLASSIFICATION OF THIS PAGE	19. SECURITY CLASSIFICATION OF ABSTRACT	20. LIMITATION OF ABSTRACT
Unclassified	Unclassified	Unclassified	UL